Model Analysis of Hypersonic Gliding Vehicle

Research Project 1 – 085851

Spring 2024

Bar Gawi

Advisors: Prof. Moshe Idan & Dr. Oded Golan

Faculty of Aerospace Engineering Technion – Israel Institute of Technology

Table of Contents

Introduction

The project centers on developing an advanced control design algorithm for Hypersonic Gliding Vehicles (HGV) which typically have nonlinear coupled dynamics and includes significant uncertainties, in cooperation with Israel Aerospace Industries (IAI). This collaboration aims to address challenges in stability and performance across various operating points within the flight envelope. The algorithm's primary goal is to maintain both stability and optimal performance across multiple defined operating points within the flight envelope. This dual requirement is crucial for achieving robust, reliable control that adapts to varying conditions. Before delving into the control design, a preliminary analysis of the model's behavior and properties is essential. This stage includes characterizing the HGV's dynamic modes and understanding how the uncertainty model impacts the system's behavior. Such an analysis provides critical insights into the system's stability boundaries and performance limitations under uncertain conditions. To support this characterization, linearizing the model around specific operating points is helpful. At this stage, we ignore the coupling between the longitudinal and lateral dynamics. However, in later stages, it will be necessary to integrate these models to fully understand the system's behavior.

Longitudinal Model

The longitudinal nonlinear ordinary differential equations (ODE) system can be expressed in the form of $\dot{\bar{x}} = f(\bar{x}, u)$, where x represents the state vector and u represents the control inputs. In this form, $f(\bar{x}, u)$ encapsulates the nonlinear dynamics governing the longitudinal behavior of the system. The system is (see reference [1])

$$\bar{x} = [\mathbb{V} \quad \alpha \quad \theta \quad Q]^T \; ; \; u = \delta_e \tag{1}$$

$$\dot{\bar{x}} = \begin{bmatrix} \dot{\mathbb{V}} \\ \dot{\alpha} \\ \dot{\theta} \\ \dot{Q} \end{bmatrix} = \begin{bmatrix} -\frac{D}{m} - g sin(\theta - \alpha) \\ -\frac{L}{m\mathbb{V}} + Q + \frac{g}{\mathbb{V}} \cos(\theta - \alpha) \\ Q \\ \frac{M}{I_y} \end{bmatrix}$$

where the aerodynamic forces and moments are defined by

$$\begin{aligned} D &= \frac{1}{2}\rho S \mathbb{V}^2 C_D(\alpha, \delta_e) \quad ; \quad C_D = -C_z(\alpha, \delta_e)\sin(\alpha) - C_x(\alpha, \delta_e)\cos(\alpha) \\ L &= \frac{1}{2}\rho S \mathbb{V}^2 C_L(\alpha, \delta_e) \quad ; \quad C_L = -C_z(\alpha, \delta_e)\cos(\alpha) + C_x(\alpha, \delta_e)\sin(\alpha) \\ M &= \frac{1}{2}\rho S L_{length} \mathbb{V}^2 C_m(\alpha, \delta_e) \end{aligned} \tag{2}$$

The aerodynamic coefficients are given as a function of the angle of attack and elevator deflection

$$C_z = C_{z_0} + C_{z_\alpha}\alpha + C_{z_{2\alpha}}\alpha^2 + C_{z_{3\alpha}}\alpha^3 + C_{z_{\delta_e}}\delta_e + C_{z_{\alpha\delta_e}}\alpha\delta_e + C_{z_{2\alpha\delta_e}}\alpha^2\delta_e + C_{z_{\alpha 2\delta_e}}\alpha\delta_e^2 + C_{z_{3\delta_e}}\delta_e^3 \tag{3}$$

$$C_x = C_{x_0} + C_{x_\alpha}\alpha + C_{x_{2\alpha}}\alpha^2 + C_{x_{3\alpha}}\alpha^3 - C_{x_{\delta_e}}|\delta_e| - C_{x_{\alpha\delta_e}}\alpha|\delta_e| - C_{x_{2\alpha\delta_e}}\alpha^2|\delta_e| + C_{x_{\alpha 2\delta_e}}\alpha\delta_e^2 - C_{x_{3\delta_e}}|\delta_e|^3 \tag{4}$$

$$C_m = C_{m_0} + C_m\alpha + C_{m_{2\alpha}}\alpha^2 + C_{m_{3\alpha}}\alpha^3 + C_{m_{\delta_e}}\delta_e + C_{m_{\alpha\delta_e}}\alpha\delta_e + C_{m_{2\alpha\delta_e}}\alpha^2\delta_e + C_{m_{\alpha 2\delta_e}}\alpha\delta_e^2 + C_{m_{3\delta_e}}\delta_e^3 \tag{5}$$

The model parameters and their uncertainties, provided by IAI, are presented in the appendix.

Equilibrium States

Currently, only one operating point has been specified, with the following parameters:

- Air density $\rho = 0.65 \frac{kg}{m^3}$
- Velocity $\mathbb{V}_0 = 1500 \frac{m}{s}$

- Angle of attack $\alpha_0 = 1.5°$
- Pitch rate $Q_0 = \text{constant}$
- Pitch moment $M = 0$

This operating point serves as a reference for initial analysis, providing a baseline for stability and performance assessments. By starting with this specific configuration, we can gain insights into the model's behavior and refine the control algorithm to accommodate varying flight conditions and uncertainties.

The trim value for the elevator deflection $\delta_{e_{trim}}$ is determined by solving the zeroed Eq.(5), given that $\alpha = \alpha_0$. Next, the nominal pitch rate Q_0 is obtained by solving the zeroed second equation of Eqs. (1). This ensures that the angle of attack α remains constant. Note that in our case, the initial pitch angle θ_0 is set to zero. Although it evolves over time since pitch rate is not zero, it has minimal effect on α. This assumption holds because the gravitational component in the equation $\dot{\alpha}$ (the rate of change of the angle of attack) is negligible in our case, where the aerodynamic forces are dominant. Additionally, the resulting effect of θ on the computed value of Q_0 is small, allowing for the simplification of the system without significantly impacting the accuracy of the pitch rate calculation. The variation in the computed pitch rate as a function of the pitch angle is depicted in Fig. 1.

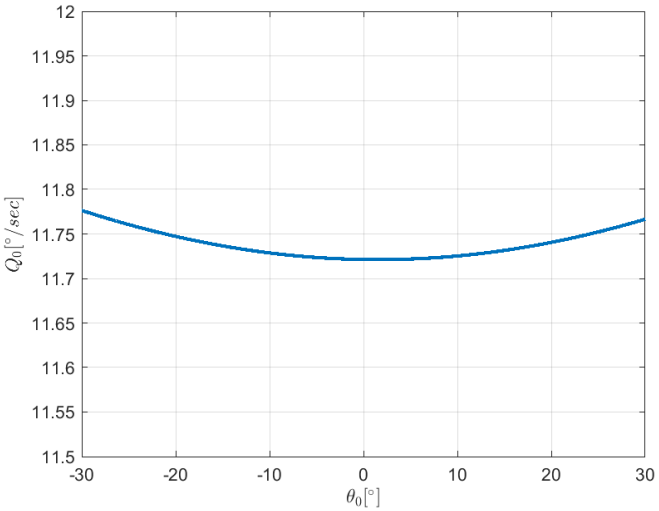

Figure 1: Computed pitch rate as a function of the pitch angle.

For the above flight condition, the resulting trim elevator deflection, $\delta_{e_{trim}}$ is found to be -14.6 degrees, and the pitch rate Q_0 is 11.7 degrees per second. During the maneuver, the longitudinal deceleration is approximately -23 [g]. The variation of this deceleration as a function of the pitch angle is depicted in Fig. 2. At the beginning of this short maneuver the perpendicular acceleration $|a_z|$ is about 30 [g] which is much larger than the contribution of the gravity term in Eq. 1. This observation suggests that the pitch rate is relatively insensitive to changes in θ_0, which could be attributed to the small impact of gravitational forces and the negligible effect of θ_0 on the pitch dynamics within the given operating conditions.

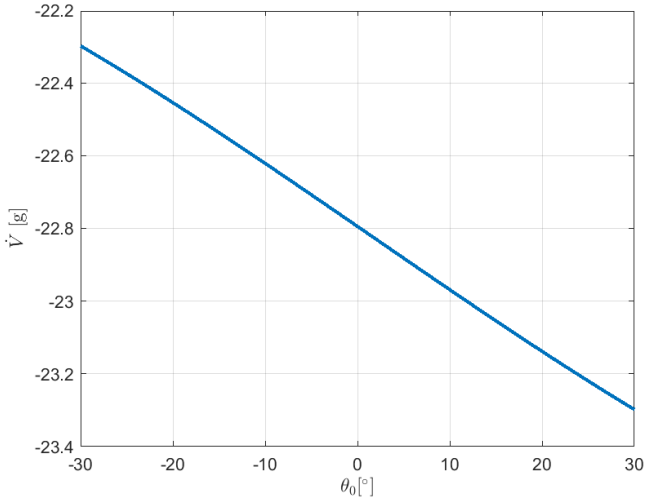

Figure 2: Longitudinal deceleration as a function of the pitch angle.

The $\delta_{e_{trim}}$ value of -14.6 degrees is considered relatively large for elevator deflection. To further assess this, over 10,000 realizations of the uncertainties in the model were performed. The resulting histogram shown in Fig. 3 indicates that the typical range for the trim elevator deflection is mostly between -12 and -17 degrees. This suggests that, while the nominal value is -14.6 degrees, the uncertainty in the model leads to a broader spread of potential deflections, about 83% falling within the -12 to -17 degree range. This variability must be taken into account when designing the control system to ensure robustness under uncertain conditions.

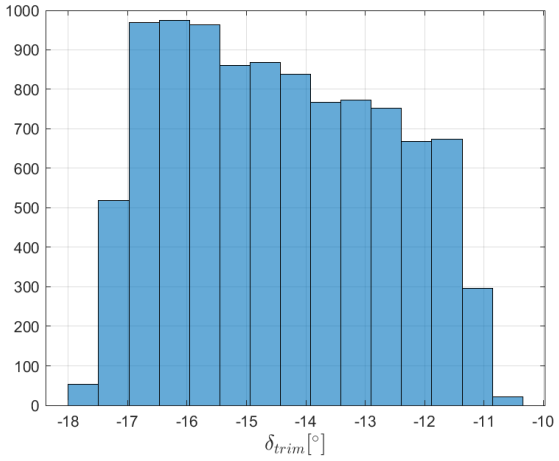

Figure 3: Histogram of elevator deflection trim angle.

Gravity Contribution

Aside from the negligible effect of θ_0 variations on the pitch rate and longitudinal deceleration, neglecting the gravitational terms in the ODEs would completely nullify the impact of θ, as it appears only in the gravitational term of the equations. Specifically, the gravity contribution in $\dot{\mathbb{V}}$ equation is $\left|\frac{mg\sin(\theta_0-\alpha_0)}{D}\right|$, and the gravity contribution in $\dot{\alpha}$ equation is $\left|\frac{mg\cos(\theta_0-\alpha_0)}{L}\right|$. The results shown in Figs. 4 and 5 indicate that the contribution of gravity in the force equations are small compared to the aerodynamic terms. Given this small effect, it can be considered negligible in the analysis and modeling. This allows for simplifying the system by excluding gravity's influence on the dynamics, ensuring that the focus remains on the more significant factors driving the system's behavior.

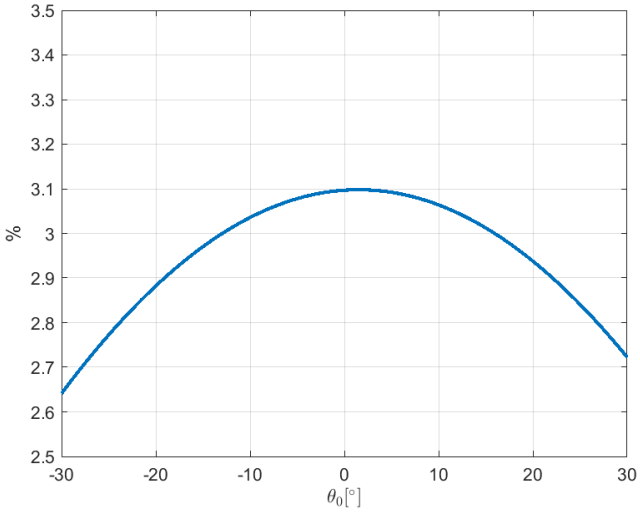

Figure 4: Contribution of the gravity term in $\dot{\alpha}$ equation.

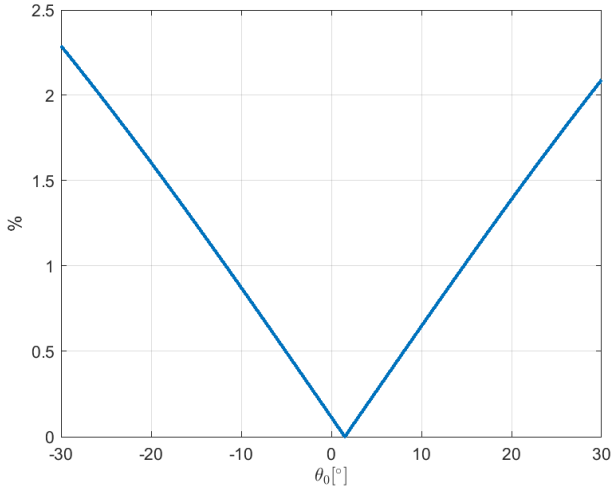

Figure 5: Contribution of the gravity term in $\dot{\mathbb{V}}$ equation.

Linearization & Results

The linearization around the equilibrium states is done numerically by

$$A(i,j) = \frac{\partial f_i}{\partial x_j}|_{x_0,u_0} \approx \frac{f_i(\bar{x}_0 + \varepsilon\bar{e}_j, \bar{u}_0) - f_i(\bar{x}_0, \bar{u}_0)}{\varepsilon} \tag{6}$$

$$B(i,j) = \frac{\partial f_i}{\partial u_j}|_{x_0,u_0} \approx \frac{f_i(\bar{x}_0, \bar{u}_0 + \varepsilon\bar{e}_j) - f_i(\bar{x}_0, u_0)}{\varepsilon}$$

where

$$\bar{e}_j = \left[0,\ 0\ , \ldots,\ \overset{j_{th}}{\overbrace{1}}\ ,\ 0\ ,\ \ldots 0\right]^T \quad ; \qquad \varepsilon \ll 1$$

and x_0 and u_0 are the trimmed values of the states and control input at the equilibrium. A is the dynamic matrix and B is the input matrix of the linearized model in the form of

$$\dot{\bar{x}} = A\bar{x} + Bu \tag{7}$$

The numeric results for the trim conditions considered in this study are

$$A = \begin{bmatrix} -0.298 & -772.8 & -9.806 & 0 \\ -1.451 \cdot 10^{-4} & -4.684 & 1.712 \cdot 10^{-4} & 1 \\ 0 & 0 & 0 & 1 \\ 0 & -784.2 & 0 & 0 \end{bmatrix}$$

$$B = \begin{bmatrix} 118.4 \\ 0.175 \\ 0 \\ 1513 \end{bmatrix}$$

Once the linearized model is obtained, the characteristic polynomial can be calculated by evaluating $\det(sI - A)$ where I the identity matrix is of the appropriate size. The roots of this polynomial are the system's eigenvalues and provides insight into the stability and dynamic behavior of the system. Mathematically, it is expressed as

$$\Delta(s) = \det(sI - A) = 0 \tag{8}$$

Solving Eq. 8 yields the eigenvalues of the system which are presented in Fig. 6. In the longitudinal model, these eigenvalues are associated with the short-period (S.P.) mode and the phugoid (energy-transfer) mode. The S.P. eigenvalues are located at $-2.34 \pm 27.9j$, meaning that the natural frequency is $\omega_n = 28 \left[\frac{1}{sec}\right]$ and the damping ratio is $\zeta = 0.083$, while the eigenvalues associated with the phugoid mode are located at -0.005 and -0.293.

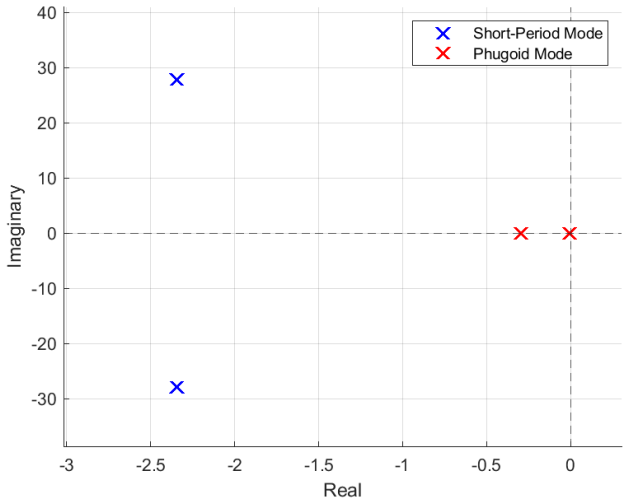

Figure 6: Longitudinal nominal eigenvalues

The eigenvalues of the system vary as a function of the system parameters which are uncertain. Fig. 7 illustrates the eigenvalues locations for some samples of parameters within the uncertainty range. From this, we observe that while the S.P. eigenvalues shift significantly, those associated with the phugoid mode exhibit minimal variation, hence allowing us to focus solely on analyzing the eigenvalues associated with the S.P. mode.

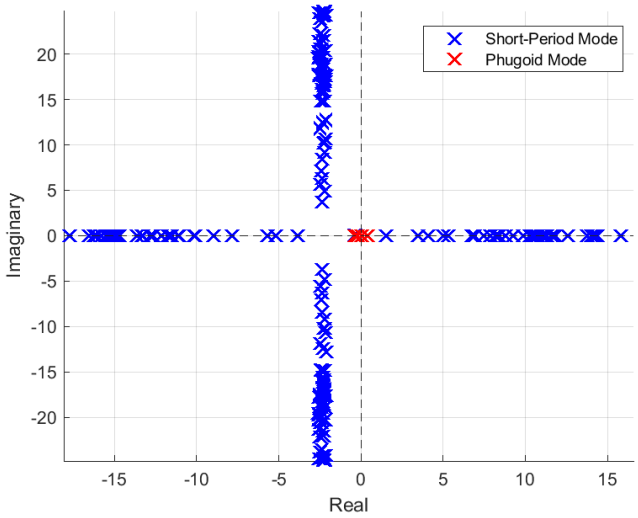

Figure 7: Longitudinal eigenvalues variation due to uncertainties

Out of the 24 possible sources of uncertainty in the longitudinal model (as outlined in the document provided by IAI), the **location of the reference point** (along the x-body axis) was identified as the most significant contributor to variations in the dynamic characteristics of the longitudinal model of the aircraft. This uncertainty, with a deviation of ±10%, directly affects the pitch moment coefficient, i.e.,

$$C_{m_{body}}{}_{scatter} = C_{m_{body}} \pm 0.1 \cdot C_{z_{body}} \tag{9}$$

The realization of this uncertainty has a significant impact on the stability and damping of the short-period mode as is depicted in Fig. 8.

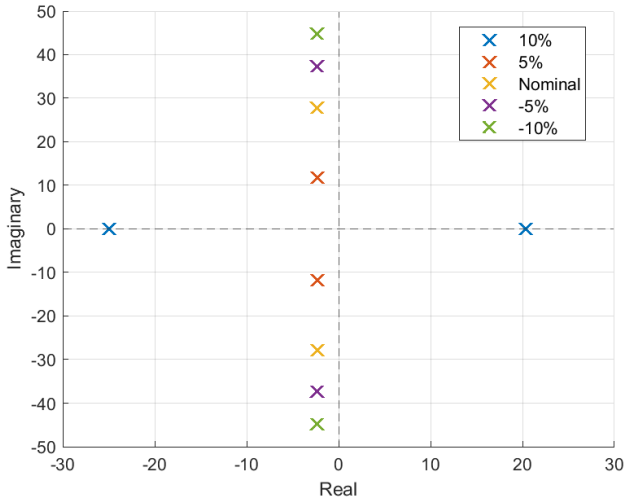

Figure 8: Short-period eigenvalues vs displacement of reference point

A scatter plot featuring thousands of realizations, representing the entire types of uncertainties (distributed uniformly) in the longitudinal model, specifically for the given deviations of the location of the reference point are presented in Fig. 9.

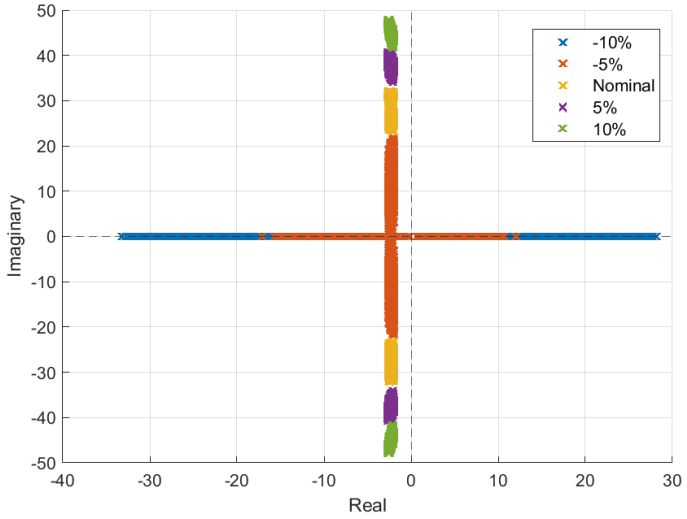

Figure 9: Short-period eigenvalues variation

Interestingly, the wide range of uncertainties in the system leads to outcomes ranging from a stable but low-damping configuration to a highly unstable system, with an unstable eigenvalue reaching magnitudes near 30 in extreme cases. This variability highlights the significant challenge in designing a robust control system capable of managing such a broad spectrum of dynamic behavior. A highly responsive control system is essential to accommodate these uncertainties, emphasizing the need for careful design to ensure stability across all scenarios.

Lateral Model

The lateral nonlinear ODE system is based on the 4 equations of the full 6-DOF model, i.e., it includes only the equations relevant to the lateral dynamics. These equations are

(10)

$$
\begin{aligned}
&m\left(\dot{V} - PW + RU - gsin(\phi)\cos(\theta_0)\right) = Y \\
&I_x\dot{P} + \left(I_z - I_y\right)RQ = L \\
&I_z\dot{R} + \left(I_y - I_x\right)PQ = N \\
&\dot{\phi} = P + Qsin(\phi)\tan(\theta) + Rcos(\phi)\tan(\theta)
\end{aligned}
$$

where

(11)

$$
\begin{aligned}
Y &= \frac{1}{2}\rho S\mathbb{V}^2 C_y(\alpha, \beta, \delta_e, \delta_a, \delta_r) \\
L &= \frac{1}{2}\rho S L_{length}\mathbb{V}^2 C_l(\alpha, \beta, \delta_e, \delta_a, \delta_r) \\
N &= \frac{1}{2}\rho S L_{length}\mathbb{V}^2 C_n(\alpha, \beta, \delta_e,\ \delta_a, \delta_r)
\end{aligned}
$$

The model parameters and their uncertainty, provided by IAI, are presented in the appendix.

Equilibrium States

In addition to the parameters specified in the longitudinal model, the equilibrium states of the lateral model are:

- Slip angle $\beta_0 = 0$
- Roll angle $\phi_0 = 0$
- Roll rate $P_0 = 0$
- Yaw rate $R_0 = 0$
- Pitch rate $Q_0 = 11.7\ [^\circ/sec]$ (obtained in the longitudinal model)

The velocity components in the body frame can be determined once the angle of attack and the slip angle are known. In the case addressed here,

$$
\begin{aligned}
U_0 &= \mathbb{V}_0 \cos(\beta_0)\cos(\alpha_0) \approx 1500\frac{m}{s} \\
V_0 &= \mathbb{V}_0 \sin(\beta_0) = 0 \\
W_0 &= \mathbb{V}_0 \cos(\beta_0)\sin(\alpha_0) \approx 40\frac{m}{s}
\end{aligned}
\tag{12}
$$

Linearization

Linearization of the lateral model can be performed numerically, similarly to the method used for the longitudinal dynamics. However, here we opted to carry out the linearization analytically, as this is the first research project, and we wanted to practice both methods to gain experience and better understand their applications. The linearization is performed by introducing small perturbations around the temporary current equilibrium states of the nonlinear model. Parameters like the Moment of Inertia $\bar{\bar{I}}$ and equilibrium conditions from the longitudinal model are included, along with the derivative coefficients provided in the full model. The linearized equations are

$$
\begin{aligned}
\dot{\beta} &= Y_v \cdot \beta + Y^{\star}_{\delta_r} \cdot \delta_r + Y^{\star}_{\delta_a} \cdot \delta_a + \frac{W_0}{\mathbb{V}_0} p - \frac{U_0}{\mathbb{V}_0} r + \frac{g\phi}{\mathbb{V}_0} cos(\theta_0) \\
\dot{p} &= L_\beta \cdot \beta + L_{\delta_r} \cdot \delta_r + L_{\delta_a} \cdot \delta_a + \frac{I_y - I_z}{I_x} Q_0 r \\
\dot{r} &= N_\beta \cdot \beta + N_{\delta r} \cdot \delta_r + N_{\delta_a} \cdot \delta_a + \frac{I_x - I_y}{I_z} Q_0 p \\
\dot{\phi} &= p + tan(\theta_0)\, r + Q_0\, tan(\theta_0)\, \phi
\end{aligned}
\tag{13}
$$

where

$$
\begin{aligned}
Y_v &= \frac{\rho S \mathbb{V}_0}{2m} C_{y_\beta} \quad ; \quad Y^{\star}_{\delta} = \frac{\rho S \mathbb{V}_0}{2m} C_{y_\delta} \\
L_\beta &= \frac{\rho S \mathbb{V}_0^2 L}{2I_x} C_{l_\beta} \; ; \quad L_\delta = \frac{\rho S \mathbb{V}_0^2 L}{2I_x} C_{l_\delta} \\
N_\beta &= \frac{\rho S \mathbb{V}_0^2 L}{2I_z} C_{n_\beta} \; ; \quad N_\delta = \frac{\rho S \mathbb{V}_0^2 L}{2I_z} C_{n_\delta}
\end{aligned}
\tag{14}
$$

The linearized model (Eqs. 13) can now be written in matrix form

$$\begin{bmatrix}\dot{\beta}\\ \dot{p}\\ \dot{r}\\ \dot{\phi}\end{bmatrix}=\underbrace{\begin{bmatrix}Y_v & tan\,(\alpha_0) & -1 & \frac{g}{\mathbb{V}_0}cos\,(\theta_0)\\ L_\beta & 0 & \frac{I_y-I_z}{I_x}Q_0 & 0\\ N_\beta & \frac{I_x-I_y}{I_z}Q_0 & 0 & 0\\ 0 & 1 & tan(\theta_0) & Q_0\,tan(\theta_0)\end{bmatrix}}_{A}\begin{bmatrix}\beta\\ p\\ r\\ \phi\end{bmatrix}+\underbrace{\begin{bmatrix}Y^*_{\delta_r} & Y^*_{\delta_a}\\ L_{\delta_r} & L_{\delta_a}\\ N_{\delta_r} & N_{\delta_a}\\ 0 & 0\end{bmatrix}}_{B}\begin{bmatrix}\delta_r\\ \delta_a\end{bmatrix} \tag{15}$$

Results

Solving Eq. 8 where the matrix A is given in Eq. 15 yields the eigenvalues of the system. The lateral model usually consists of three known modes. The Dutch-roll mode (which is analogous to the short-period mode in the longitudinal model) has a pair of complex eigenvalues, the roll mode has a single real eigenvalue and is fast and highly damped, and the spiral mode has a single real eigenvalue and is typically very slow and can be stable or unstable. However, the resulting eigenvalues, presented in Fig. 10, indicate that our nominal case is atypical, perhaps due to the complexity of the model. All four eigenvalues are real, with one of them being very unstable. In fact, it is not clear which of the eigenvalues corresponds to which mode. Later, we will discuss how the modes behave to gain better insight.

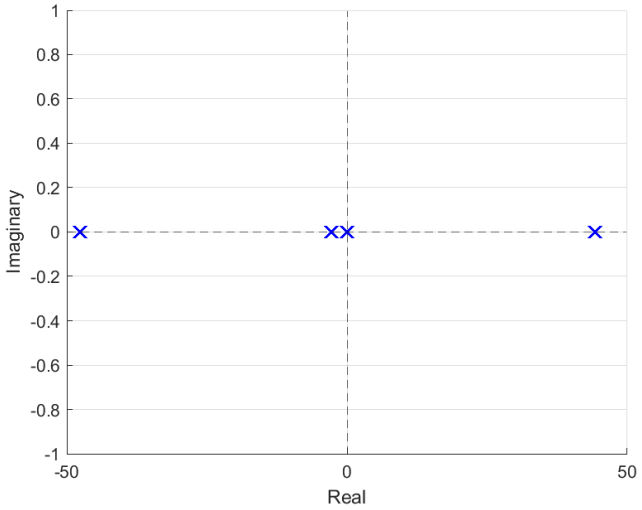

Figure 10: Lateral nominal eigenvalues

Similarly to the longitudinal model, the dominant uncertainty (in terms of dynamic characteristics of the lateral model) arises from deviations in the location of the reference point, as is reflected in the yaw moment coefficient with respect to the slip angle β,

$$C_{n_\beta}{}_{scatter} = C_{n_\beta} \mp 0.1 \cdot C_{y_\beta} \tag{16}$$

Effectively, C_{n_β} becomes less negative as the reference point deviates forward, resulting in increasing stability, and vice versa. The results are presented in Figs. 11 and 12.

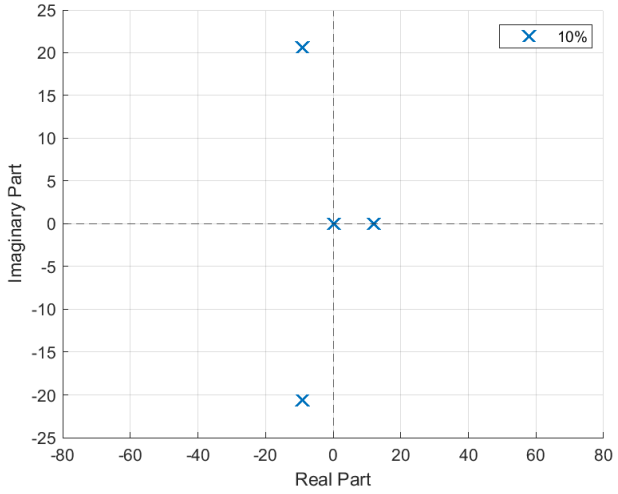

Figure 11: Lateral eigenvalues when reference point deviates forward

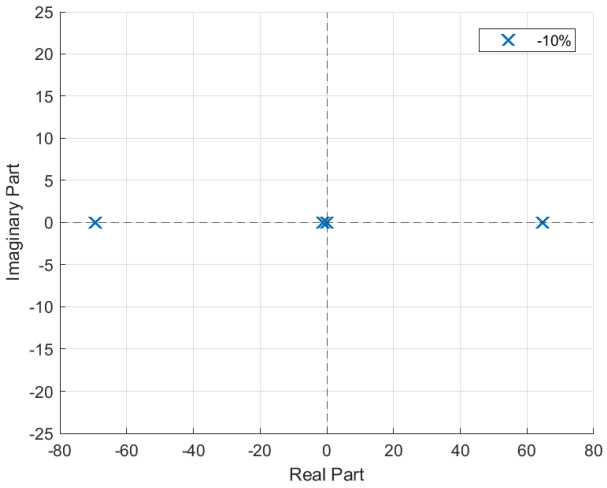

Figure 12: Lateral eigenvalues when reference point deviates backward

A scatter plot featuring thousands of realizations, representing the different types of uncertainties (distributed uniformly) in the lateral model, specifically for the deviations of the location of the reference point is shown in Fig. 13.

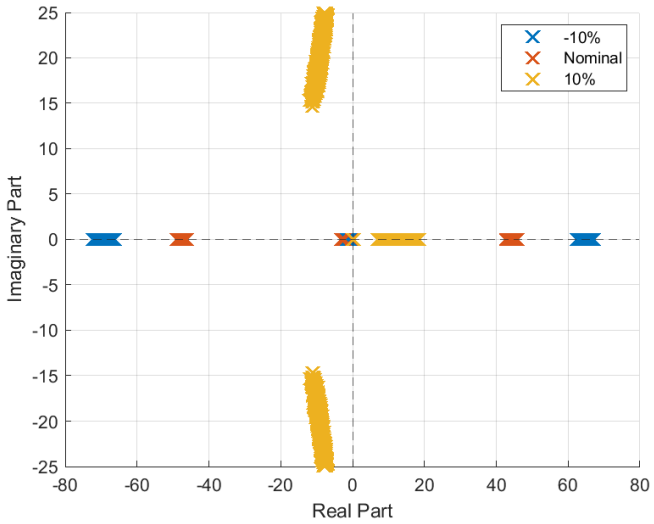

Figure 13: Scattered lateral eigenvalues

The presence of uncertainties results in varying degrees of instability in the system. It is clear that the lateral model is always unstable, with eigenvalues consistently in the right half-plane. The primary variation lies in the severity of the instability, reflected by how far to the right the eigenvalues are located. Note that in both the longitudinal and lateral models, shifting the reference point forward enhances stability (in this case, decreasing instability).

Modes Analysis

Recall that the nominal eigenvalues, as shown in Fig. 10, are not as typical as we would expect. To analyze them, we can examine the eigenvectors corresponding to each eigenvalue. The components of the eigenvectors reveal how state variables, such as roll, yaw, and sideslip, contribute to each mode. This approach helps identify the dominant motion in each mode and provides insight into how the states interact. Tables 1-3 summarize the results for each case (displacement of the reference point). Note that the order of the values in each vector corresponds to the order of the states, which is

$$\bar{x} = [\beta\ p\ r\ \phi]^T \tag{17}$$

Eigenvalue	**-47.65**	**44.39**	**-2.896**	**-0.0002**
Eigenvector	0.0015	-0.0014	0.0001	0
	-0.999	-0.998	-0.945	-0.002
	0.0355	-0.0435	-0.0229	0.0065
	0.021	-0.0225	0.3263	1

Table 1: Nominal case

Eigenvalue	**-69.58**	**64.83**	**-1.42**	**-0.0005**
Eigenvector	0.002	-0.002	0	0
	-0.993	-0.993	-0.817	-0.0005
	0.11	0.116	-0.017	0.0065
	0.014	-0.015	0.576	1

Table 2: Reference point deviated backward

Eigenvalue	**-8.92±20.53j**	**11.693**	**0.002**
Eigenvector	-0.0003±0.006j	0.0004	0
	0.998	0.996	0.0002
	0.0384±0.0072j	0.02	0.006
	-0.0178±0.041j	0.085	1

Table 3: Reference point deviated forward

The dominant components of the eigenvectors presented in the tables above are marked. Notably, the roll rate p dominates these modes. One potential explanation for this is the absence of rate derivatives in the model, particularly L_p, which typically accounts for roll damping. This means, for example, that the Dutch-roll mode, which normally consists of sideslip and yaw rate, is characterized by roll rate in our case.

Summary

This initial phase of the research focused on gaining a deeper understanding of the dynamic model provided by Israel Aerospace Industries (IAI). The primary goal was to begin uncovering key behaviors in the model, including the response of the longitudinal and lateral modes under specified operating conditions. By examining uncertainties, analyzing characteristic eigenvalues, and evaluating the roles of various parameters, we have established a foundation for future work. Given that this is an early stage, adjustments and refinements are anticipated as we receive updates from the industry and hold future discussions with IAI. This flexible approach will ensure that the model remains aligned with evolving project goals.

References

[1] Parker, J. T., Bolender, M. A., & Doman, D. B. (2005). Control-oriented modeling of an air-breathing hypersonic vehicle. *Journal of Guidance, Control, and Dynamics, 28*(5), 886–894.

Appendix

The appendix includes Tables 4 and 5, which detail the relevant model parameters and properties discussed in this report.

Aerodynamic Coefficient	Polynomial Coefficient	Value	Deviation
$C_{m_{control}}$	C_{m_δ}	0.035	$\pm 10\%$
	$C_{m_{\alpha\delta}}$	0.06	
	$C_{m_{2\alpha\delta}}$	1.7	
	$C_{m_{\alpha 2\delta}}$	-2.8	
	$C_{m_{3\delta}}$	0.5	
$C_{z_{body}}$	C_{z_0}	-0.03	
	C_{z_α}	-2.25	
	$C_{z_{2\alpha}}$	0	
	$C_{z_{3\alpha}}$	-2	
$C_{z_{control}}$	C_{z_δ}	0.02	
	$C_{z_{\alpha\delta}}$	0.035	
	$C_{z_{2\alpha\delta}}$	0.5	
	$C_{z_{\alpha 2\delta}}$	0.55	
	$C_{z_{3\delta}}$	0.35	
$C_{x_{body}}$	C_{x_α}	-0.07	
	$C_{x_{2\alpha}}$	-0.5	
	$C_{x_{3\alpha}}$	-1	
	C_{x_0}	-0.06	
$C_{x_{control}}$	C_{x_δ}	0.008	
	$C_{x_{\alpha\delta}}$	-0.017	
	$C_{x_{2\alpha\delta}}$	0.3	
	$C_{x_{\alpha 2\delta}}$	0.2	
	$C_{x_{3\delta}}$	0.15	
C_{l_β}	$C_{l_{\beta_0}}$	0.25	
	$C_{l_{\beta\alpha}}$	-0.6	
C_{y_β}	$C_{y_{\beta 0}}$	-3.2	
	$C_{y_{\beta\alpha}}$	13.6	
$C_{n_{\delta_r}}$	$C_{n_{\delta_{r_0}}}$	0.04	
	$C_{n_{\delta_r\alpha}}$	-0.15	
$C_{l_{\delta_a}}$	$C_{l_{\delta_a\delta}}$	-1.2	
	$C_{l_{\delta_a\alpha}}$	0.03	
$C_{l_{\delta_r}}$	$C_{l_{\delta_r 0}}$	-0.01	$\pm 20\%$
	$C_{l_{\delta_r\alpha}}$	0.06	
$C_{n_{\delta_a}}$	$C_{n_{\delta_a\delta}}$	0.4	
	$C_{n_{\delta_a\alpha}}$	0.04	
	$C_{n_{\delta_a}\delta\alpha}$	13.5	
$C_{y_{\delta_a}}$	$C_{y_{\delta_a 0}}$	0.013	
	$C_{y_{\delta_a\delta}}$	-2	
	$C_{y_{\delta_a\alpha}}$	-0.04	

Table 4: Model's aerodynamic coefficients and uncertainties

Property	Value	Units
Mass	450	$[Kg]$
Ixx	125	$[Kg \cdot m^2]$
Iyy	125	
Izz	130	
Surface	2	$[m^2]$
Length	0.75	$[m]$

Table 5: Model's properties